

Dalton Transactions

Accepted Manuscript



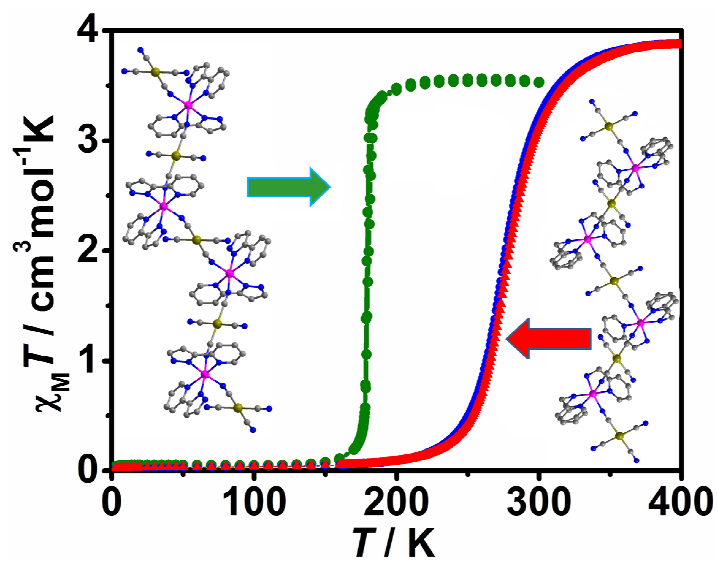
This is an *Accepted Manuscript*, which has been through the Royal Society of Chemistry peer review process and has been accepted for publication.

Accepted Manuscripts are published online shortly after acceptance, before technical editing, formatting and proof reading. Using this free service, authors can make their results available to the community, in citable form, before we publish the edited article. We will replace this *Accepted Manuscript* with the edited and formatted *Advance Article* as soon as it is available.

You can find more information about *Accepted Manuscripts* in the [Information for Authors](#).

Please note that technical editing may introduce minor changes to the text and/or graphics, which may alter content. The journal's standard [Terms & Conditions](#) and the [Ethical guidelines](#) still apply. In no event shall the Royal Society of Chemistry be held responsible for any errors or omissions in this *Accepted Manuscript* or any consequences arising from the use of any information it contains.

Table of Content



Four one-dimensional heterobimetallic spin crossover coordination polymers $\{\text{Fe}(L)_2[\text{M}(\text{CN})_4]\}_n$ ($M = \text{Pd}^{\text{II}}$ and Pt^{II}) have been synthesized and characterized.

ARTICLE

Spin Crossover Behaviour in One-Dimensional Fe^{II} Compounds Based on the [M(CN)₄]²⁻ (M = Pd, Pt) Units

Cite this: DOI: 10.1039/x0xx00000x

Shao-Liang Zhang, Xin-Hua Zhao, Yuan-Min Wang, Dong Shao and Xin-Yi Wang*

Received 00th January 2012,
Accepted 00th January 2012

DOI: 10.1039/x0xx00000x

www.rsc.org/

Four one-dimensional heterobimetallic coordination polymers {Fe(pic)₂[M(CN)₄]}_n (M = Pd^{II} (1) and Pt^{II} (2), pic = 2-picolyamine), and {Fe(pypz)₂[M(CN)₄]}_n (M = Pd^{II} (3) and Pt^{II} (4), pypz = 2-(1H-pyrazol-3-yl)pyridine) have been synthesized and characterized by infrared spectroscopy, X-ray diffraction, magnetic measurements and differential scanning calorimetry (DSC). Single-crystal X-ray analyses show that all the compounds are 1D neutral zigzag chain structures in which the planar [M(CN)₄]²⁻ anion acts as a μ -bridging ligand, and the two pic/pypz molecules as chelating coligands. Examination of the intermolecular contacts in compounds 1 - 4 reveals the existence of the hydrogen bonding interactions involving the hydrogen donor groups of the pic and pypz ligands and the nitrogen atoms of the non-bridging cyanide groups of the [M(CN)₄]²⁻ anions. Weak π - π interactions were also found to be important for the formation of the 3D structures for compounds 3 and 4. The SCO properties of all compounds were confirmed by the detailed structural analyses of the coordination environments of the Fe^{II} centres, DSC analyses, and magnetic susceptibility measurements. Compounds 1 and 2 exhibit complete SCO behaviour with very narrow thermal hysteresis loops centred near the room temperature ($T_{1/2} \downarrow = 270$ K and $T_{1/2} \uparrow = 272$ K for 1 and $T_{1/2} \downarrow = 272$ K and $T_{1/2} \uparrow = 274$ K for 2), whereas 3 and 4 exhibit abrupt SCO at 186 and 180 K, respectively. Compared to the mononuclear species of the pic and pypz ligands, the SCO temperatures are adjusted by the different ligand field strength of the [M(CN)₄]²⁻ units. The cooperativity from both the coordination bonds and supramolecular interaction leads to the observation of the hysteresis loops in the Fe-pic systems and the abrupt SCO transition in the Fe-pypz systems. Furthermore, the light-induced excited-spin-state trapping (LIESST) effect was observed for 2.

Introduction

Spin-crossover (SCO), a spin-switching phenomenon which usually takes place for octahedrally coordinated 3d transition metal ions of 4 to 7 electrons (d^4 – d^7), has been extensively explored in the field of molecular magnetism.¹ Under an appropriate ligand field strength, their electron configurations can be reversibly switched between the low-spin and high-spin states by external stimuli such as temperature, pressure, light irradiation, guest molecules absorption/desorption and so on.² Such a process is usually accompanied by changes in physical properties such as magnetism, colour, fluorescence, dielectric constant and so on.³ Hence, SCO materials are of great potential for the applications in sensing, data storage, information processing and display devices.⁴

As most of the materials with bistability, the major parameters for the SCO materials are the working temperature

and the hysteresis effect. For practical application, which is very difficult for most of the other molecular magnetic materials, the wide thermal hysteresis loop centred at around room temperature is very appealing and widely pursued.⁵ For this purpose, the appropriate ligand field strength and cooperative effect are the key ingredients. Although the basic physics of SCO behaviour can be understood in the framework of ligand field theory, it is still very difficult to predict and even tailor the SCO property of a new compound. The main reason is the lack of knowledge to control the cooperative effects. For most of the reported SCO materials, which are discrete mononuclear compounds,⁶ weak supramolecular interactions, such as the hydrogen bonding, π - π interaction, and van der Waals interactions, are the most important sources of the cooperativity. Compared to these weak, and often barely controllable supramolecular interactions, the stronger coordination bonds not only give more reliable control on the structures with higher dimensionality, but also usually lead to

more efficient cooperative effects and enhanced SCO properties.^{2d,2e,7} As an illustrative example, the one dimensional (1D) Fe^{II}-1,2,4-triazole coordination polymers where the Fe^{II} centres were bridged together by the triazole ligands show remarkable cooperative SCO transition accompanied by wide hysteretic loops at around room temperature.⁸ Besides, in these SCO coordination polymers, the weak supramolecular interactions is also of great importance as it can greatly adjust the SCO properties, such as the $T_{1/2}$ value and width of hysteretic loops.⁸⁻⁹ This is also nicely demonstrated by several very interesting 2D (such as the {Fe(SCN)₂(azpy)₂}·solvent, azpy = 4,4'-azobispyridine)^{9a} or 3D (such as the 3D Hofmann type {Fe(pyrazine)₂[M(CN)₄]}·solvent)^{9b-9d,2e} coordination polymers where the solvent molecules have a huge and controllable impact on the SCO properties.

For the construction of the extended SCO coordination polymers, the bridging ligands are of great importance. Besides the bisonodentate ligands such as the triazole and azpy mentioned above, the cyano ligands, including both the organocyanates (like the dicyanamide,^{10a} tricyanomethanide,^{10b} 7,7,8,8-tetracyano-quinodimethane^{10c} and so on) and the cyanometallates ([M(CN)_n]^{m-} and [ML(CN)_n]^{m-} groups),^{2e,10d} are of special interest. The N atoms of these anions can easily coordinated to the adjacent metal centres and are of suitable ligand field strength; the cyanometallate building blocks are usually rigid enough to induces strong cooperativity; the multiple CN groups in the cyanometallates are very promising to form high dimensional structures; and importantly, the cyanometallates can be paramagnetic, which can lead to very interesting magnetic materials with SCO centres being bridged by the paramagnetic centres. At low temperature, magnetic properties can be judiciously adjusted by the LIESST effect of the SCO centres and remarkable results including the photo-induced single-chain magnets^{10d,11a} and photomagnets^{11b-11e} were reported.

On the other hand, for the synthesis of these cyanometallate bridged SCO coordination polymers, suitable ancillary ligands are usually involved. The most widely used ancillary ligands include the monodentate heterocyclic ligands such as the pyridine and their derivatives,¹² the bisonodentate ligands such as pyrazine,^{9b-9d} pyrimidine,^{13a-b} bpe,^{13c} azpy^{13d} and so on.^{2e} The usage of the bidentate or multidentate ligands with pyridine groups in the construction of SCO compounds with extended structures is somehow limited. Among the various bidentate ligands, we are interested in the 2-picolylamine (pic) and 2-(1H-pyrazol-3-yl)pyridine (pypz) as they are of great importance to the study of Fe^{II}-SCO compounds. The study of the SCO properties of the [Fe(pic)₃]·anion-solvent compounds can be traced back to 1960's and had an important impact on study of the Fe^{II} SCO properties.¹⁴ Remarkably, the SCO properties of these compounds can be finely tuned by different counter ions and solvent molecules incorporated in the structure.¹⁴ At the same time, the SCO properties of the pypz and a large number of the related ligands were also widely investigated.¹⁵ By combining these bidentate ligands and the [M(CN)₄]²⁻ (M = Pd, Pt) anions, we were able to isolate four 1D

compounds where the bidentate ligands chelated Fe^{II} centres were bridged by the [M(CN)₄]²⁻ building blocks. Up to now, the 1D SCO coordination polymers based on cyano ligands remain scarcely reported. The reported examples include the following: [Fe(L)₂(AgCN)₂]·Solvent (L = bpt⁻, Mebpt⁻, and bpzt⁻),^{16a} {Fe(Mebpt)[Au(CN)₂]}_n·xH₂O^{16b}, [Fe(abpt)₂][C[C(CN)₂]₃]^{16c}, {Fe(abpt)₂[M(CN)₄]} (M = Pt and Ni),^{16d} {Fe(aqin)₂[M(CN)₄]} (M = Ni(II), Pt(II),^{16e} {Fe(aqin)₂[N(CN)₂]}(ClO₄)·MeOH,^{10a} {Fe(3-CNpy)₂[Cu(3-CNpy)(μ-CN)₂]_n},^{16f} and [Fe(L_{N3O2})(CN)₂][Mn(hfac)₂].^{16g} Herein, we report the syntheses, structures, and magnetic properties of these 1D compounds. To the best of our knowledge, these systems are the first examples of the 1D SCO chain compounds based on the Fe-pic and Fe-pypz building blocks. Single crystal X-ray diffractions at both high and low temperatures, magnetic measurements, and DSC analyses on these compounds revealed the persistence of the SCO behaviour of all four compounds. As anticipated, these 1D compounds show significant cooperative effects as confirmed by the hysteresis loops and LIESST effect for the Fe-pic compounds and the abrupt spin transition for the Fe-pypz compounds.

Experimental Section

Physical Measurements

Elemental analyses of carbon, hydrogen, and nitrogen were carried out on a Vario EL II Elementar. Infrared spectral samples were prepared as KBr pellets and the spectra were obtained on a Bruker Tensor 27 FT-IR spectrometer. Powder X-ray diffraction (PXRD) were recorded at 298 K on a Bruker D8 Advance diffractometer with Cu Kα X-ray source (operated at 40 kV and 40 mA). DSC measurements were recorded using a METTLER-TOLEDO DSC1 differential scanning calorimeter with temperature sweep rate of 10 K min⁻¹. Magnetic measurements were carried out using a Quantum Design SQUID VSM magnetometer on the freshly prepared samples for all the compounds at temperatures ranging from 2 to 400 K under a dc field of 1000 Oe. Experimental susceptibilities were corrected for diamagnetism of the sample holders and that of the compounds according to Pascal's constants.

Materials and Preparations of Compounds 1-4

All reagents used in this work were obtained from commercial sources (analytical reagent grade) without further purification. All the operations for the synthesis were carried out in deoxygenated solvents under a nitrogen atmosphere using glove box techniques to avoid the oxidation of Fe^{II} ion. **{Fe(pic)₂[Pd(CN)₄]}_n (1).** An H-shaped tube was charged with a 3 mL of H₂O–MeOH (v : v = 2 : 1) solution containing 21 mg of FeSO₄·7H₂O (0.075 mmol) and 18 mg of pic (0.165 mmol) in one side and 2 mL of water solution containing 77 mg of K₂Pd(CN)₄·3H₂O (0.225 mmol) in the other side. Another 4 mL of H₂O–MeOH (v : v = 1 : 1) solvent was carefully added to the top of the solutions as a buffer. The tube was then sealed and stored in the dark. Brown single crystals formed in three

weeks. The crystals were removed from the H-tube and washed with methanol. Yield: 22.8 mg, 63%. Elemental analysis (%) calculated for $C_{16}H_{16}N_8FePt$: C, 39.82; H, 3.34; N, 23.22. Found: C, 39.63; H, 3.51; N, 23.10. IR (cm^{-1}): 2161(s) and 2135(s) for $\nu(C\equiv N)$.

{Fe(pic)₂[Pt(CN)₄]}_n (2). This compound was prepared by a similar procedure as that of **1** using $K_2Pt(CN)_4 \cdot 3H_2O$ (97 mg, 0.225 mmol). Yield: 25.3 mg, 59%. Elemental analysis (%) calculated for $C_{16}H_{16}N_8FePt$: C, 33.64; H, 2.82; N, 19.61. Found: C, 33.59; H, 3.12; N, 19.54. IR (cm^{-1}): 2159(s) and 2133(s) for $\nu(C\equiv N)$.

{Fe(pypz)₂[Pd(CN)₄]}_n (3). This compound was prepared by a similar slow diffusion procedure as that of **1** using $FeSO_4 \cdot 7H_2O$

(21 mg, 0.075 mmol), pypz (24 mg, 0.165 mmol), and $K_2Pd(CN)_4 \cdot 3H_2O$ (77 mg, 0.225 mmol). Yellow single crystals formed in three weeks. Yield: 22.0 mg, 53%. Elemental analysis (%) calculated for $C_{20}H_{12}N_{10}FePd$: C, 43.30; H, 2.18; N, 25.25. Found: C, 42.91; H, 2.24; N, 25.10. IR (cm^{-1}): 2156(s) for $\nu(C\equiv N)$.

{Fe(pypz)₂[Pt(CN)₄]}_n (4). This compound was prepared by a similar procedure as that of **3** using 97 mg of $K_2Pt(CN)_4 \cdot 3H_2O$. Yield: 24.1 mg, 50%. Elemental analysis (%) calculated for $C_{20}H_{12}N_{10}FePt$: C, 37.34; H, 1.88; N, 21.77. Found: C, 37.05; H, 2.38; N, 21.68. IR (cm^{-1}): 2153(s) for $\nu(C\equiv N)$.

Table 1. Crystallographic data and structure refinement parameters for compounds **1-4**.

complex	1		2		3		4	
formula	$C_{16}H_{16}N_8FePt$		$C_{16}H_{16}N_8FePt$		$C_{20}H_{14}N_{10}FePd$		$C_{20}H_{14}N_{10}FePt$	
formula weight	482.62		571.31		556.66		645.35	
<i>T</i> / K	120	298	120	298	120	298	120	298
crystal system	monoclinic		monoclinic		monoclinic		monoclinic	
space group	<i>P</i> 2 ₁ / <i>c</i>	<i>P</i> 2 ₁ / <i>c</i>	<i>P</i> 2 ₁ / <i>m</i>	<i>P</i> 2 ₁ / <i>c</i>	<i>C</i> 2/ <i>c</i>	<i>C</i> 2/ <i>c</i>	<i>C</i> 2/ <i>c</i>	<i>C</i> 2/ <i>c</i>
<i>a</i> / Å	10.0448(11)	10.2201(11)	7.8428(6)	10.2838(11)	14.255(3)	14.377(3)	14.269(3)	14.304(3)
<i>b</i> / Å	15.2279(16)	15.6565(16)	15.2262(12)	15.6772(16)	10.247(2)	10.470(2)	10.366(2)	10.523(2)
<i>c</i> / Å	15.6122(12)	15.9375(12)	8.4043(7)	16.0125(12)	14.539(3)	15.253(4)	14.532(4)	15.157(4)
α / deg	90.00	90.00	90.00	90.00	90.00	90.00	90.00	90.00
β / deg	125.869(4)	126.500(4)	103.3670(10)	126.470(4)	99.489(4)	102.588(4)	99.222(4)	102.323(4)
γ / deg	90.00	90.00	90.00	90.00	90.00	90.00	90.00	90.00
<i>V</i> / Å ³	1935.2(3)	2050.0(3)	976.42(13)	2076.00(3)	2094.8(8)	2241.0(9)	2121.7(9)	2228.9(9)
<i>Z</i>	4	4	2	4	4	4	4	4
<i>F</i> (000)	960	960	544	1088	1104	1104	1232	1232
collected refl.	17154	18089	6875	13175	9008	7510	8699	7442
unique refl.	4417	4698	1772	4405	2404	2588	2420	2575
<i>R</i> _{int}	0.1431	0.0337	0.0394	0.0214	0.0456	0.0395	0.0587	0.0230
<i>R</i> ₁ ^a / <i>wR</i> ₂ ^b	0.0438,0.1183	0.0290,0.0737	0.0264,0.0769	0.0247,0.0757	0.0308,0.0721	0.0322,0.0660	0.0286,0.0635	0.0174,0.0379
(<i>I</i> > 2 σ (<i>I</i>))								
GOF	1.019	1.044	1.226	1.036	1.044	1.005	1.013	1.004

$$^a R_1 = \sum ||F_o| - |F_c|| / \sum |F_o|. \quad ^b wR_2 = \{ \sum [w(F_o^2 - F_c^2)^2] / \sum [w(F_o^2)^2] \}^{1/2}$$

Table 2. Selected bond lengths (Å) and structural parameters of **1-4** at various temperatures.

	1 (120 K)	1 (298 K)	2 (120 K)	2 (298 K)	3 (120 K)	3 (298 K)	4 (120 K)	4 (298 K)			
Fe1-N1	1.948(3)	2.112(2)	Fe1-N1	1.928(4)	Fe1-N1	2.129(4)	Fe1-N1	1.952(2)	2.141(3)	1.951(4)	2.139(2)
Fe1-N3	1.928(2)	2.088(2)	Fe1-N4	1.975(6)	Fe1-N3	2.102(3)	Fe1-N3	1.986(2)	2.190(2)	1.994(4)	2.186(2)
Fe1-N5	1.972(3)	2.152(2)	Fe1-N5	2.028(17)	Fe1-N5	2.160(4)	Fe1-N4	1.953(2)	2.185(2)	1.962(4)	2.182(2)
Fe1-N6	2.032(2)	2.189(2)	Fe1-N6	1.964(17)	Fe1-N6	2.210(3)					
Fe1-N7	1.967(2)	2.157(2)	Fe1-N7	2.008(7)	Fe1-N7	2.165(4)					
Fe1-N8	2.020(3)	2.188(3)			Fe1-N8	2.191(4)					
Fe-N _{av}	1.977	2.147	1.981	2.159	1.964	2.172	1.969	2.169			
CShM	0.353	0.923	0.499	0.967	0.468	1.008	0.462	0.993			
$\sum Fe$	38.71	58.11	46.64	59.70	49.14	66.88	48.26	66.91			
Θ	59.32	91.12	65.14	93.20	86.96	102.51	77.19	100.01			

CShM: continuous shape measure relative to ideal octahedron; $\sum Fe$: the sum of the deviation from 90° of the 12 *cis*-angles of the FeN_6 octahedron, Θ : the sum of the deviation from 60° of the 24 trigonal angles of the projection of the FeN_6 octahedron onto its trigonal faces.

X-ray Data Collection and Structure Refinement

X-ray data for compounds **1-4** were collected on a Bruker APEX DUO diffractometer with a CCD area detector (Mo-K α radiation, $\lambda = 0.71073$ Å) under nitrogen at 298 and 120 K, respectively. The APEXII program was used to determine the

unit cell parameters and for data collection. Data were integrated using SAINT¹⁷ and SADABS.¹⁸ The structures of all the compounds were solved by direct methods and refined by full matrix least-squares methods based on F^2 using the SHELXTL program.¹⁹ Anisotropic thermal parameters were used for the non-hydrogen atoms. Hydrogen atoms of the

organic ligands were refined as riding on the corresponding non-hydrogen atoms. Single-crystal X-ray diffraction and refinement details are given in Table 1. Selected bond lengths, structural parameters and bond angles for complexes 1-4 are given in Table 2 and Tables S1-S4.

Results and Discussion

Crystal Structure Descriptions

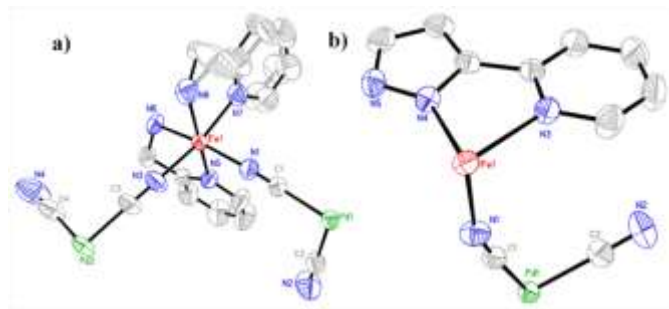


Figure 1. The asymmetry units of **1** (a) and **3** (b) at 298 K, rendered with 50% probability ellipsoids. Hydrogen atoms were omitted for clarity.

As the ligands pic and pypz both act as bidentate ligands, the structures of compounds **1-4** are very similar to each other, although they crystallize in different space groups. All of them crystallize in the monoclinic crystal system (Table 1). The space group of **1**, **3**, and **4** remain the same at both 120 and 298 K ($P2_1/c$ for **1** and $C2/c$ for **3** and **4**), while it changes from $P2_1/m$ at 120 K to $P2_1/c$ at 298 K for **2**. For all four compounds, there is no lattice solvent molecule. At 298 K, the asymmetric units of **1** and **2** consist of one Fe^{II} centre surrounded by two pic in a general position and two half of the $[\text{M}(\text{CN})_4]^{2-}$ units located in the inversion centre; while for **3** and **4**, there are only half of the Fe^{II} centre, one pypz ligand, and half of the $[\text{M}(\text{CN})_4]^{2-}$ unit in the asymmetry unit (Figure 1). Each Fe^{II} ion is six-coordinated by four nitrogen atoms from two pic or pypz ligands and two nitrogen atoms from two $[\text{M}(\text{CN})_4]^{2-}$ species in a *cis* arrangement. As for the square-planar $[\text{M}(\text{CN})_4]^{2-}$ units ($\text{M} = \text{Pd}^{\text{II}}$ and Pt^{II}), the M-C and C-N bond lengths are in the normal range. Using two of the *trans* CN^- groups, the $[\text{M}(\text{CN})_4]^{2-}$ units connected the Fe^{II} ions forming the 1D zig-zag chains along the *b* axis for **1** and **2** and *c* axis for **3** and **4**, respectively (Figure 2).

In addition, structural disorder was found in both compounds **1** and **2**. For **1**, one of the pic ligands was disordered over two positions at both temperatures (Figure 1). The situation is somehow strange for compound **2**. Although the high temperature structure of **2** is isostructural to **1**, we cannot get a satisfied refinement for the low temperature phase at 120 K using the same space group $P2_1/c$. However, the refinement goes well with the space group $P2_1/m$ and a different unit cell which is half of that for the high temperature phase (Table 1). Also, we tried several different single crystals of **2** and the situation remained the same. For the low

temperature phase of **2**, both the $\text{Fe}(\text{II})$ and $\text{Pt}(\text{II})$ centers are located in the special positions, which lead to the disorder of the whole $[\text{Pt}(\text{CN})_4]^{2-}$ unit and the two pic ligands over two positions (Figure 3). Because of the reduced unit cell, the disorder of the low temperature phase of **2** reflects the superposition of the adjacent $[\text{Fe}(\text{pic})_2]^{2+}$ and $[\text{Pt}(\text{CN})_4]^{2-}$ units in the unit cell of the high temperature phase (see Figure 3 and 4b for comparison).

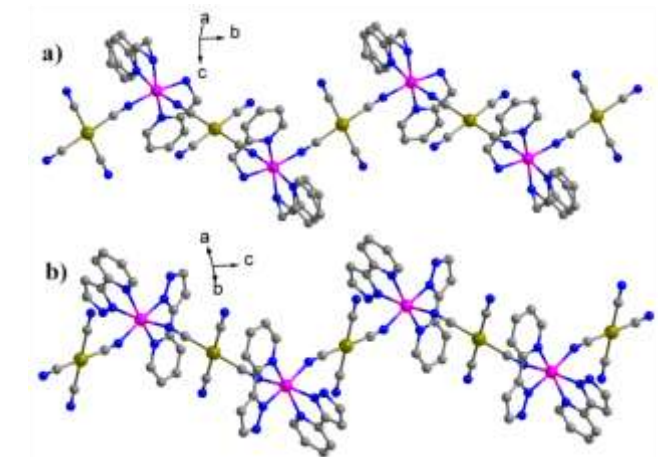


Figure 2. The 1D zig-zag chain structure of compounds **1** (a) and **3** (b).

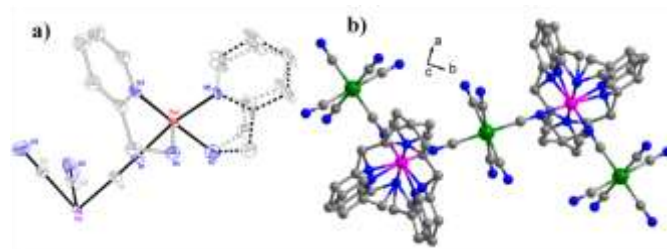


Figure 3. The asymmetry unit (a) (showing 50% probability ellipsoids) and 1D zig-zag chain structure of compound **2** at 120 K. Hydrogen atoms were omitted for clarity.

At 298 K, the average Fe-N distances are 2.147, 2.159, 2.172, and 2.169 Å for **1-4**, respectively. These values decrease to 1.977, 1.981, 1.964 and 1.969 Å at 120 K, respectively. The decrease of the average Fe-N bond length is consistent with the spin crossover transition from high-spin to low-spin Fe^{II} centres (vide post), as the depopulation of the anti-bonding e_g^* orbitals leads to the strengthening of the Fe-N bonds. Besides the change of the Fe-N bond lengths, the coordination environment of Fe^{II} is significantly modified at two different temperatures during the spin transition. At both 120 and 298 K, several structure parameters, including the continuous shape measures (CShM's) relative to the ideal octahedron calculated using the program SHAPE 2.1,²⁰ the parameters Σ (the sum of the deviation from 90° of the 12 *cis*-angles of the FeN_6 octahedron) and Θ (the sum of the deviation from 60° of the 24 trigonal angles of the projection of the FeN_6 octahedron onto its trigonal faces) were calculated and listed in Table 2. As can be seen, all

the CShM's, Σ , and Θ parameters observed at room temperature are significantly larger than those at 120 K, indicative of the high degree of distortion of the FeN_6 octahedrons at 298 K and more regular octahedral geometry at 120 K. The changes of these parameters are consistent with the SCO transition^{16c} and are also in line with the spin-state assignments of these four compounds as can be seen below in the magnetic properties.

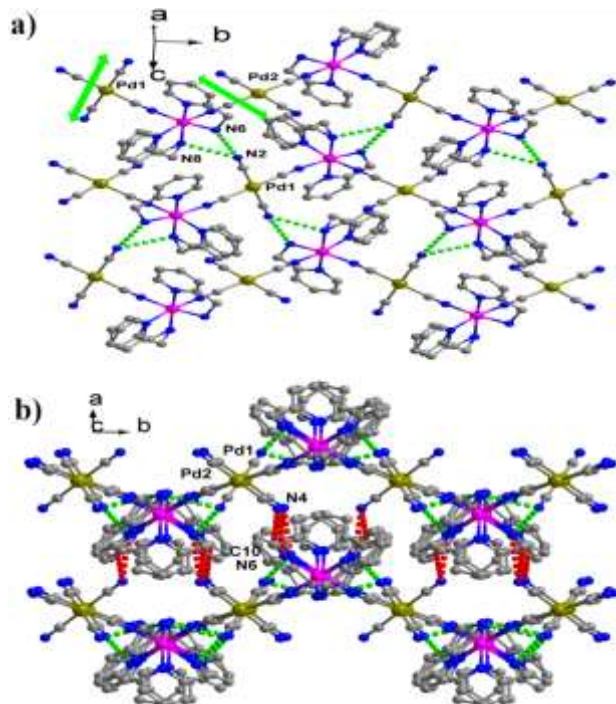


Figure 4. The 2D layer (a) and 3D structure (b) of **1** constructed from the hydrogen bond interactions. The arrows in (a) denote the different directions of the two terminal CN^- groups of adjacent $[\text{Pd}(\text{CN})_4]^{2-}$ units along the chain; and the dashed lines with different colours represent the different hydrogen bonds involving the terminal CN^- groups.

As the spin crossover properties are usually very sensitive to the supramolecular interactions such as the hydrogen bonding and π - π interaction, we carefully examined the structures of **1-4** to identify these weak interactions. Although the 1D chains of **1** and **2** are very similar to those of **3** and **4**, the alignments of these chain to 3D structures are significantly different, resulting from different supramolecular interactions. The main interchain contacts observed for all four compounds at both 298 and 120 K are gathered in Table 3. As we can see in Figure 4, the $[\text{M}(\text{CN})_4]^{2-}$ units in **1** and **2** are twisted to each other along the chain so that the two terminal CN^- groups of the adjacent $[\text{M}(\text{CN})_4]^{2-}$ units point to two different directions. However for **3** and **4**, all the terminal CN^- groups of the $[\text{M}(\text{CN})_4]^{2-}$ units are roughly parallel to each other (Figure 5). As these terminal CN^- groups are responsible for the interchain hydrogen bonds, these differences lead to the different packing schemes. For **1** and **2**, the chains first linked to each other by the $\text{N-H}\cdots\text{N}$ hydrogen bonds between the NH_2 groups from the pic ligands and the N2 atom of the terminal CN^- group from Pd1/Pt1, forming 2D layers along the bc plane (Figure 4a).

Along the a axis, these layers were further connected to each other by another set of $\text{N-H}\cdots\text{N}$ and $\text{C-H}\cdots\text{N}$ hydrogen bonds involving the N4 atoms of the terminal CN groups from Pd2/Pt2 (Figure 4b). On the other hand for **3** and **4**, the 1D chains interact to each other by the π - π interactions between the pypz ligands and form 2D layers along the bc plane (Figure 5a). These layers were linked together by the $\text{N-H}\cdots\text{N}$ hydrogen bonds between N2 atom of the $[\text{M}(\text{CN})_4]^{2-}$ and the NH group of the pypz ligand, forming the 3D structure (Figure 5b).

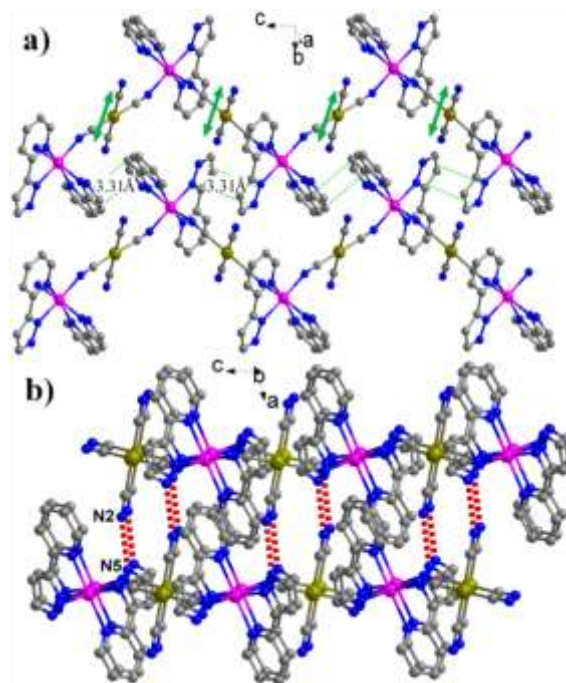


Figure 5. The 2D layer along the bc plane (a) and 3D structure (b) of **3** constructed from the interchain π - π interactions (green dashes) and the hydrogen bond interactions (red dashes).

Table 3. Hydrogen bonding and π - π interactions [\AA] at two temperatures for complexes **1-4**.

T / K	Complex 1		Complex 2	
	D...A	d(D...A) / \AA	D...A	d(D...A) / \AA
120	N6...N2a	3.075(3)	N5...N2c	3.150(2)
	N8...N2a	3.154(3)	C4...N2c	3.112(2)
	N6...N4b	3.152(4)	N5...N3d	3.080(2)
	C10...N4b	3.092(4)		
298	N6...N2a	3.097(3)	N6...N2a	3.121(5)
	N8...N2a	3.218(4)	N8...N2a	3.288(6)
	N6...N4b	3.170(4)	N6...N4b	3.184(6)
	C10...N4b	3.179(4)	C10...N4b	3.198(7)
120	Complex 3		Complex 4	
	D...A	d(D...A) / \AA	D...A	d(D...A) / \AA
120	N5...N2e	2.807(3)	N5...N2e	2.824(6)
	π - π	3.250(2)	π - π	3.262(2)
298	N5...N2e	2.827(4)	N5...N2e	2.822(4)
	π - π	3.340(2)	π - π	3.340(3)

Symmetry codes: a: $x, -y+3/2, z+1/2$; b: $-x+1, -y+1, -z+1$; c: $x+1, y, z+1$; d:

$x+1, y, z$; e: $x+1/2, y+1/2, z$.

Magnetic Properties and Thermal Analysis

The magnetic properties of **1–4** were measured with temperature up to 400 K in 1 kOe. In the case of **1** and **2** (Figure 6a and 6b), the $\chi_M T$ value is 3.79 and 3.88 $\text{cm}^3\text{mol}^{-1}\text{K}$ at 400 K, confirming the HS state of the hexacoordinated Fe^{II} centres. Upon cooling to 300 K, the $\chi_M T$ value decrease gradually down to 3.22 and 3.21 $\text{cm}^3\text{mol}^{-1}\text{K}$. Upon further cooling, the $\chi_M T$ values drop steeply to 0.15 and 0.09 $\text{cm}^3\text{mol}^{-1}\text{K}$ at 200 K, showing the HS-LS SCO transition. At the lowest temperature of 2 K, the $\chi_M T$ values are very close to zero (0.012 and 0.012 $\text{cm}^3\text{mol}^{-1}\text{K}$ for **1** and **2**, respectively), indicating the complete SCO transition from high spin $S = 2$ to a diamagnetic low spin $S = 0$ state. In addition, under a temperature sweep rate of 10 K/min, two subsequent cooling–heating cycles provide the presence of very narrow thermal hysteresis loops with the width of 2 K for **1** and **2** centred at a temperature a little bit lower than the room temperature ($T_{1/2\downarrow} = 270$ K and $T_{1/2\uparrow} = 272$ K for **1**, $T_{1/2\downarrow} = 272$ K and $T_{1/2\uparrow} = 274$ K for **2**). These loops were also observed with narrower widths under a slower temperature sweep rate of 1 K/min and 5 K/min (Figure S10, S11). Furthermore, the LIESST effect of **2** was explored by applying green light (532 nm) to irradiate the sample to saturation at 2 K for 5 h. The maximum $\chi_M T$ value at 2 K (0.25 $\text{cm}^3\text{K mol}^{-1}$) indicated that a photoexcited population of approximately 6.4% HS Fe^{II} ion was achieved. The presence of the narrow hysteresis in both compounds and also the LIESST effect of **2** suggest the cooperative effect of **1** and **2**, which can be attributed to the 1D coordination polymer and existence of the weak intermolecular interactions.

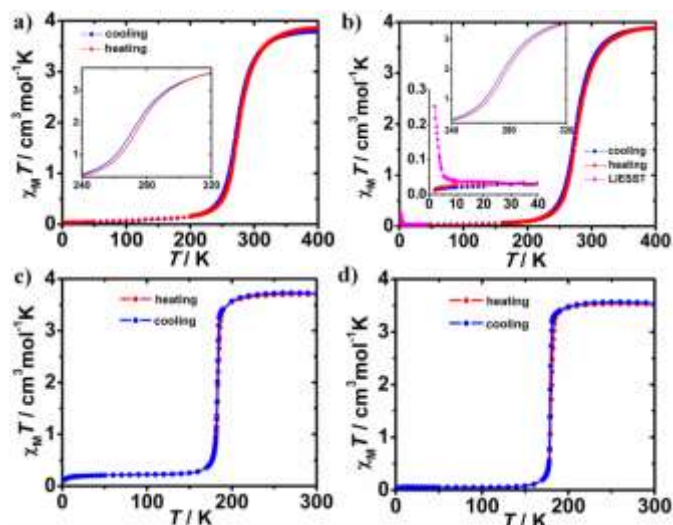


Figure 6. Temperature dependent $\chi_M T$ plots for **1** (a), **2** (b), **3** (c), and **4** (d). Inset: the expansion of the hysteresis loops and the LIESST effect of **2**.

For complexes **3** and **4**, the magnetic properties are also similar to each other (Figure 6c and 6d). The $\chi_M T$ values observed at room temperature are about 3.71 and 3.51 $\text{cm}^3\text{mol}^{-1}\text{K}$, respectively. The values are consistent with a $S = 2$ HS state of the octahedral $\text{Fe}(\text{II})$ ions. Upon cooling, the $\chi_M T$

values remain constant, down to a temperature of about 195 K for **3** and 190 K for **4**. Below these temperatures, the sharp decrease indicates the occurrence of an abrupt HS-LS SCO transition. Below 100 K, the $\chi_M T$ values are close to 0 $\text{cm}^3\text{mol}^{-1}\text{K}$, implying the complete SCO transition. The curve of the warming process is nearly identical to that of the cooling one, that is, no hysteresis is observed. The critical temperatures are 186 and 180 K for **3** and **4**, respectively. No LIESST effect was observed in **3** and **4**.

Furthermore, to detect the thermally induced SCO transitions in **1–4**, differential scanning calorimetry (DSC) measurements were performed. As shown in Figure 7, upon heating/cooling at 10 K/min, heat anomalies of endothermic/exothermic peaks were observed at $\sim 270/268$, $274/272$, $187/187$, and $179/179$ K for **1–4**, respectively. These peak temperatures agree well with the SCO transition temperatures observed in the magnetic measurements. The corresponding ΔH values were estimated to be 3.00/–4.02, 7.16/–6.39, 6.95/–8.22, and 8.38/–8.95 kJmol^{-1} for **1–4**. The corresponding ΔS values were estimated to be 11.1/–15.0, 26.2/–23.6, 37.2/–43.9, and 46.8/–50.0 $\text{JK}^{-1}\text{mol}^{-1}$ for **1–4**. These values are within the experimental range generally observed for the Fe^{II} SCO complexes.^{3e}

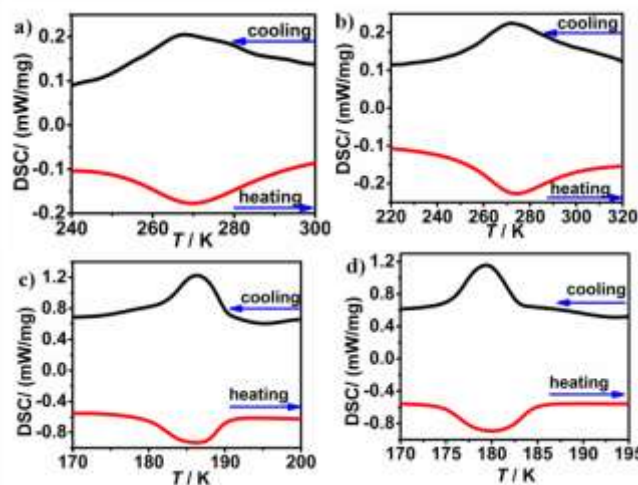


Figure 7. DSC curves of **1** (a), **2** (b), **3** (c), and **4** (d). The heating and cooling modes are in red and black lines, respectively.

Comparison of the SCO properties of 1-4 with their mononuclear analogues.

As mentioned in the Introduction part, the pic and pypz ligands have been the major players in the field of SCO compounds. The mononuclear compounds based on these ligands with the general composition $[\text{Fe}(\text{L})_3](\text{X})_2 \cdot \text{solvent}$ have offered many great examples for the study of the effect of the anions and solvents on the SCO properties (Table 4). Comparison of the SCO properties of these mononuclear analogues to compounds **1–4** should be of value to better understand the SCO properties of these systems. For the $[\text{Fe}(\text{pic})_3](\text{X})_2 \cdot \text{solvent}$ compounds, there are two different

geometries of the $[\text{Fe}(\text{pic})_3]^{2+}$ centre: *mer*- $[\text{Fe}(\text{pic})_3]^{2+}$ for most of the reported compounds^{14a-f} and *fac*- $[\text{Fe}(\text{pic})_3]^{2+}$ for the *fac*- $[\text{Fe}(\text{pic})_3\text{Cl}_2]\cdot x\text{H}_2\text{O}$ and half of the Fe^{II} centers in $[\text{Fe}(\text{pic})_3]\text{I}_2$.^{14f-g} The hydrogen bond interactions were found to be critical to the SCO properties of these compounds, especially for the *fac*- $[\text{Fe}(\text{pic})_3\text{Cl}_2]\cdot x\text{H}_2\text{O}$ species.^{14f-h}

Table 4 Summary of the SCO properties of $[\text{Fe}(\text{L})_3](\text{X})_2\cdot\text{solvent}$ (L = pic and pypz) mononuclear complexes.

$[\text{Fe}(\text{pic})_3](\text{X})_2\cdot\text{solvent}$				
complex	Solvent	$T_{1/2}$ / K	transition type	references
<i>mer</i> - $[\text{Fe}(\text{pic})_3]\text{Cl}_2$	methanol	150	gradual	14a, 14g
	ethanol	118	two steps, gradual	14a-b, 14d-e
	allyl alcohol	124	two steps, gradual	14a
	2-propanol	147	two steps, small hysteresis	14a, 14c, 14d
	1-propanol	no	HS	14a
	tert-butyl alcohol	no	HS	14a
<i>mer</i> - $[\text{Fe}(\text{pic})_3]\text{Br}_2$	methanol	120	gradual	14e
	ethanol	123	small hysteresis	14e
<i>fac</i> - $[\text{Fe}(\text{pic})_3]\text{Cl}_2$	no solvent ^a	115	complete	14h
	H_2O^b	204, 295	hysteresis	14f, 14j
	$2\text{H}_2\text{O}$	no	LS	14f, 14g
$[\text{Fe}(\text{pic})_3]\text{I}_2^b$	no solvent	no	LS	14i
$[\text{Fe}(\text{pypz})_3](\text{X})_2\cdot\text{solvent}$				
complex		$T_{1/2}$ / K	transition type	reference
$[\text{Fe}(\text{pypz})_3](\text{BF}_4)_2\cdot\text{H}_2\text{O}$		196	incomplete	15a
$[\text{Fe}(\text{pypz})_3](\text{BF}_4)_2\cdot 1.5\text{H}_2\text{O}$		295	incomplete	15a
$[\text{Fe}(\text{pypz})_3](\text{ClO}_4)_2\cdot\text{H}_2\text{O}$		235	incomplete	15a
$[\text{Fe}(\text{pypz})_3](\text{ClO}_4)_2\cdot 3\text{H}_2\text{O}$		275	incomplete	15a
$[\text{Fe}(\text{pypz})_3](\text{PF}_6)_2\cdot 2\text{H}_2\text{O}$		323	incomplete	15a
$[\text{Fe}(\text{pypz})_3](\text{CF}_3\text{SO}_3)_2\cdot 2\text{H}_2\text{O}$		> 353	incomplete	15b
$[\text{Fe}(\text{pypz})_3](\text{CF}_3\text{SO}_3)_2$		229, 241	hysteresis	15b

^a No crystal structure for these two compounds had been reported. We assume they have the *fac*-geometry from their preparation; ^b For this compound, the $[\text{Fe}(\text{pic})_3]^{2+}$ cations of both the *mer*- and *fac*-geometry were found in the same crystal structure.

As can be seen in Table 4, except for *fac*- $[\text{Fe}(\text{pic})_3\text{Cl}_2]\cdot x\text{H}_2\text{O}$ ($x = 1$ and 2), the $T_{1/2}$ values of the $[\text{Fe}(\text{pic})_3]^{2+}$ compounds are generally lower than 150 K, which is lower than those of compounds **1** and **2**. On the other hand, for the $[\text{Fe}(\text{pypz})_3]^{2+}$ compounds, the transition temperatures are usually higher than 200 K, which are also higher than those of **3** and **4**. The change of the $T_{1/2}$ values may be ascribed to the different ligand-field strength caused by the two cyanide groups of $[\text{M}^{\text{II}}(\text{CN})_4]^{2-}$. It seems that the ligand field strength of the cyanide group of $[\text{M}^{\text{II}}(\text{CN})_4]^{2-}$ is stronger than that of the pic ligand and weaker than that of the pypz ligand. Also, except for compounds *fac*- $[\text{Fe}(\text{pic})_3\text{Cl}_2]\cdot\text{H}_2\text{O}$ and $\text{Fe}(\text{L})_3(\text{CF}_3\text{SO}_3)_2$ which were prepared from the dehydration of the hydrated samples and had no structural details, the spin transitions are generally gradual with few compounds showing very small hysteresis

loops. By introducing the bridging ligands to connect the metal centres, the cooperative effect between the metal centres could be improved. As described above, complexes **1** and **2** undergo a complete spin crossover with a small hysteresis loop and LIESST effect was observed in **2**. Compounds **3** and **4** also undergo abrupt and complete SCO behaviour. Together with the interchain supramolecular interactions, the coordination links are believed to play an important role in the cooperativity of the system.

Conclusions

In summary, we have reported here the syntheses, structures at both high and low temperatures, and magnetic properties of the four 1D Fe^{II} SCO compounds $[\text{Fe}(\text{L})_2(\mu_2\text{-M}(\text{CN})_4)]_n$ (L = pic and pypz; M = Pd^{II} and Pt^{II}). In the structure, the $[\text{Fe}(\text{L})_2]^{2+}$ units were connected by the two *trans* CN^- groups of the $\mu_2\text{-}[\text{M}(\text{CN})_4]^{2-}$ moieties, forming the 1D zig-zag chains. Those chains were further connected to each other by the weak intermolecular interactions. Structural analyses at both the HS and LS states revealed the substantial structural modifications of the local coordination environments of the Fe^{II} centres accompanied with the SCO transition. Magnetic measurements showed that **1** and **2** undergo complete SCO with narrow thermal hysteresis loops near the room temperature, while **3** and **4** exhibit abrupt SCO at around 180 K. LIESST effect was observed for compound **2**. Compared to the mononuclear $[\text{Fe}(\text{L})_3](\text{X})_2\cdot\text{solvent}$ species of the pic and pypz ligands, the spin transition temperatures are adjusted by the different ligand field strength of the $[\text{M}(\text{CN})_4]^{2-}$ units. The cooperativity in these 1D coordination polymers should result from both the coordination links and supramolecular interactions. Our results confirmed the advantages of the cyanometallates for the preparation of the new SCO compounds. Further efforts will be aimed at the new SCO materials based on the other cyanometallates, especially the paramagnetic and anisotropic cyanometallates such as the $[\text{Mo}(\text{CN})_7]^{4-}$ unit, for the construction of multifunctional magnetic materials.

Acknowledgements

We thank the Major State Basic Research Development Program (2013CB922102), NSFC (91022031, 21101093, 21471077). This work was also supported by a Project Funded by the Priority Academic Program Development of Jiangsu Higher Education Institutions. We thank Prof. Tao Liu from Dalian University of Technology in China for the LIESST measurements.

Notes and references

State Key Laboratory of Coordination Chemistry, Collaborative Innovation Centre of Advanced Microstructures, School of Chemistry and Chemical Engineering, Nanjing University, Nanjing, 210093, China. Fax: +86-25-83314502. E-mail: wangxy66@nju.edu.cn
CCDC 1050970-1050977 contain the supplementary crystallographic data for this paper. These data can be obtained free of charge from the

Cambridge Crystallographic Data Centre
via www.ccdc.cam.ac.uk/data_request/cif.

†Electronic Supplementary Information (ESI) available: Structure information in detail and powder XRD spectra. For ESI and crystallographic data in CIFs see DOI: 10.1039/b000000x/.

- (a) P. Gütllich and H. A. Goodwin, Eds. Spin Crossover in Transition Metal Compounds I, II and III. *Topics in Current Chemistry*; Springer-Verlag: Berlin, 2004; Vols. **233–235**; (b) M. A. Halcrow, *Spin-crossover materials: properties and applications*; John Wiley & Sons, Ltd.: New York, 2013; (c) K. S. Murray, H. Oshio, and J. A. Real, Eds. Special Issue on Spin-Crossover Complexes, *Eur. J. Inorg. Chem.* 2013, **5-6**, 574-1067.
- (a) P. Gütllich, A. B. Gaspar, Y. Garcia, *Beilstein J. Org. Chem.* 2013, **9**, 342-391; (b) J. Tao, R. J. Wei, R. B. Huang, L. S. Zheng, *Chem. Soc. Rev.* 2012, **41**, 703-737; (c) A. Bousseksou, G. Molnar, L. Salmon, W. Nicolazzi, *Chem. Soc. Rev.* 2011, **40**, 3313-3335; (d) J. A. Real, A. B. Gaspar and M. C. Muñoz, *Dalton Trans.*, 2005, 2062-2079; (e) M. C. Muñoz, J. A. Real, *Coord. Chem. Rev.* 2011, **255**, 2068-2093.
- (a) O. Sato, J. Tao, Y. Z. Zhang, *Angew. Chem. Int. Ed.* 2007, **46**, 2152-2187; (b) M. A. Halcrow, *Chem. Soc. Rev.* 2011, **40**, 4119-4142; (c) J. Olguín, S. Brooker, *Coord. Chem. Rev.* 2011, **255**, 203-240; (d) P. Gamez, J. Sánchez-Costa, M. Quesada, G. Aromí, *Dalton Trans.*, 2009, 7845-7853; (e) P. Gütllich, A. Hauser and H. Spiering, *Angew. Chem., Int. Ed.*, 1994, **33**, 2024-2054.
- (a) O. Kahn, C. J. Martinez, *Science*, 1998, **279**, 44-48; (b) O. Sato, *Acc. Chem. Res.* 2003, **36**, 692-700; (c) H. Tokoro, S. Ohkoshi, *Dalton Trans.* 2011, **40**, 6825-6833.
- (a) I. Šalitraš, N. T. Madhu, R. Boča, J. Pavlik, M. Ruben, *Monatsh. Chem.* 2009, **140**, 695-733; (b) M. A. Halcrow, *Chem. Lett.* 2014, **43**, 1178-1188.
- (a) B. Weber, W. Bauer, J. Obel, *Angew. Chem. Int. Ed.* 2008, **47**, 10098-10101; (b) F. El Hajj, G. Sebki, V. Patinec, M. Marchivie, S. Triki, H. Handel, S. Yefsah, R. Tripier, C. J. Gomez-Garcia, E. Coronado, *Inorg. Chem.* 2009, **48**, 10416-10423; (c) C. F. Sheu, S. Pillet, Y. C. Lin, S. M. Chen, I. J. Hsu, C. Lecomte, Y. Wang, *Inorg. Chem.* 2008, **47**, 10866-10874.
- (a) B. Weber, *Coord. Chem. Rev.* 2009, **253**, 2432-2449; (b) Y. Bodenthin, G. Schwarz, Z. Tomkowicz, M. Lommel, T. Geue, W. Haase, H. Möhwald, U. Pietsch, D. G. Kurth, *Coord. Chem. Rev.* 2009, **253**, 2414-2422; (c) S. Benmansour, C. Atmani, F. Setifi, S. Triki, M. Marchivie, C. J. Gómez-García, *Coord. Chem. Rev.* 2010, **254**, 1468-1478; (d) G. Aromí, L. A. Barrios, O. Roubeau, P. Gamez, *Coord. Chem. Rev.* 2011, **255**, 485-546.
- (a) O. Roubeau, *Chem. Eur. J.* 2012, **18**, 15230-15244; (b) J. Kröber, E. Codjovi, O. Kahn, F. Grolière, C. Jay, *J. Am. Chem. Soc.* 1993, **115**, 9810-9811.
- (a) G. J. Halder, C. J. Kepert, B. Moubaraki, K. S. Murray, J. D. Cashion, *Science* 2002, **298**, 1762-1765; (b) M. Ohba, K. Yoneda, G. Agustí, M. C. Munoz, A. B. Gaspar, J. A. Real, M. Yamasaki, H. Ando, Y. Nakao, S. Sakaki, S. Kitagawa, *Angew. Chem. Int. Ed.* 2009, **48**, 4767-4771; (c) P. D. Southon, L. Liu, E. A. Fellows, D. J. Price, G. J. Halder, K. W. Chapman, B. Moubaraki, K. S. Murray, J. F. Letard, C. J. Kepert, *J. Am. Chem. Soc.* 2009, **131**, 10998-11009; (d) X. Bao, H. J. Shepherd, L. Salmon, G. Molnar, M. L. Tong, A. Bousseksou, *Angew. Chem. Int. Ed.* 2013, **52**, 1198-1202.
- (a) C. Genre, E. Jeanneau, A. Bousseksou, D. Luneau, S. A. Borshch, G. S. Matouzenko, *Chem. Eur. J.* 2008, **14**, 697-705; (b) G. Dupouy, M. Marchivie, S. Triki, J. Sala-Pala, J. Y. Salaun, C. J. Gomez-Garcia, P. Guionneau, *Inorg. Chem.* 2008, **47**, 8921-8931; (c) H. Phan, S. M. Benjamin, E. Steven, J. S. Brooks, M. Shatruk, *Angew. Chem. Int. Ed.* 2015, **54**, 823-827; (d) T. Liu, H. Zheng, S. Kang, Y. Shiota, S. Hayami, M. Mito, O. Sato, K. Yoshizawa, S. Kanegawa, C. Duan, *Nat. Commun.* 2013, **4**, 2826-2832.
- (a) N. Hoshino, F. Iijima, G. N. Newton, N. Yoshida, T. Shiga, H. Nojiri, A. Nakao, R. Kumai, Y. Murakami, H. Oshio, *Nat. Chem.* 2012, **4**, 921-926; (b) S. Ohkoshi, K. Imoto, Y. Tsunobuchi, S. Takano, H. Tokoro, *Nat. Chem.* 2011, **3**, 564-569; (c) A. Mondal, Y. Li, L. M. Chamoreau, M. Seuleiman, L. Rechinat, A. Bousseksou, M. L. Boillot, R. Lescouezec, *Chem. Commun.* 2014, **50**, 2893-2895; (d) A. Mondal, Y. Li, P. Herson, M. Seuleiman, M. L. Boillot, E. Riviere, M. Julve, L. Rechinat, A. Bousseksou, R. Lescouezec, *Chem. Commun.* 2012, **48**, 5653-5655; (e) E. Heintze, F. El Hallak, C. Clauss, A. Rettori, M. G. Pini, F. Totti, M. Dressel, L. Bogani, *Nat. Mater.* 2013, **12**, 202-206.
- (a) V. Martínez, A. B. Gaspar, M. C. Muñoz, G. V. Bukin, G. Levchenko, J. A. Real, *Chem. Eur. J.* 2009, **15**, 10960-10971; (b) M. Sereydyuk, A. B. Gaspar, V. Ksenofontov, M. Verdagner, F. Villain, P. Gütllich, *Inorg. Chem.* 2009, **48**, 6130-6141; (c) T. Kitazawa, Y. Gomi, M. Takahashi, M. Takeda, M. Enomoto, A. Miyazaki, T. Enoki, *J. Mater. Chem.* 1996, **6**, 119-121.
- (a) A. Galet, M. C. Munoz, A. B. Gaspar, J. A. Real, *Inorg. Chem.* 2005, **44**, 8749-8755; (b) V. Niel, A. L. Thompson, A. E. Goeta, C. Enachescu, A. Hauser, A. Galet, M. C. Munoz, J. A. Real, *Chem. Eur. J.* 2005, **11**, 2047-2060; (c) F. J. Munoz-Lara, A. B. Gaspar, M. C. Munoz, M. Arai, S. Kitagawa, M. Ohba, J. A. Real, *Chem. Eur. J.* 2012, **18**, 8013-8018; (d) G. Agustí, S. Cobo, A. B. Gaspar, G. Molnar, N. O. Moussa, P. A. Szilagyí, V. Palfi, C. Vieu, M. C. Munoz, J. A. Real, A. Bousseksou, *Chem. Mater.* 2008, **20**, 6721-6732.
- (a) M. Hostettler, K. W. Tornroos, D. Chernyshov, B. Vangdal, H. B. Burgi, *Angew. Chem. Int. Ed.* 2004, **43**, 4589-4594; (b) D. Chernyshov, M. Hostettler, K. W. Tornroos, H. B. Burgi, *Angew. Chem. Int. Ed.* 2003, **42**, 3825-3830; (c) K. W. Tornroos, M. Hostettler, D. Chernyshov, B. Vangdal, H. B. Burgi, *Chem. Eur. J.* 2006, **12**, 6207-6215; (d) D. Chernyshov, B. Vangdal, K. W. Törnroos, H. B. Bürgi, *New J. Chem.* 2009, **33**, 1277-1282; (e) A. M. Greenaway, C. J. O'Connor, A. Schrock, E. Sinn, *Inorg. Chem.* 1979, **18**, 2692-2695; (f) M. Sorai, J. Enslin, K. M. Hasselbach, P. Gütllich, *Chem. Phys.* 1977, **20**, 197-208; (g) A. M. Greenaway, E. Sinn, *J. Am. Chem. Soc.* 1978, **100**, 8080-8084; (h) G. A. Renovitch, W. A. Baker, *J. Am. Chem. Soc.* 1967, **89**, 6377-6378; (i) B. A. Katz, C. E. Strouse, *Inorg. Chem.* 1980, **19**, 658-665; (j) T. Nakamoto, A. Bhattacharjee, M. Sorai, *Bull. Chem. Soc. Jpn.* 2004, **77**, 921-932.
- (a) K. H. Sugiyarto, H. A. Goodwin, *Aust. J. Chem.* 1988, **41**, 1645-1663; (b) L. S. Harimanow, K. H. Sugiyarto, D. C. Craig, M. L. Scudder, H. A. Goodwin, *Aust. J. Chem.* 1999, **52**, 109-122; (c) B. A. Leita, B. Moubaraki, K. S. Murray, J. P. Smith, J. D. Cashion, *Chem. Commun.* 2004, 156-157; (d) B. A. Leita, B. Moubaraki, K. S. Murray, J. P. Smith, *Polyhedron* 2005, **24**, 2165-2172.
- (a) Z. Yan, J. Y. Li, T. Liu, Z. P. Ni, Y. C. Chen, F. S. Guo, M. L. Tong, *Inorg. Chem.* 2014, **53**, 8129-8135; (b) Z. Yan, Z. P. Ni, F. S.

- Guo, J. Y. Li, Y. C. Chen, J. L. Liu, W. Q. Lin, D. Aravena, E. Ruiz, M. L. Tong, *Inorg. Chem.* 2014, **53**, 201-208; (c) G. Dupouy, S. Triki, M. Marchivie, N. Cosquer, C. J. Gomez-Garcia, S. Pillet, E. Bendeif el, C. Lecomte, S. Asthana, J. F. Letard, *Inorg. Chem.* 2010, **49**, 9358-9368; (d) R. Herchel, Z. Trávníček, R. Zbořil, *Inorg. Chim. Acta* 2011, **365**, 458-461; (e) F. Setifi, E. Milin, C. Charles, F. Thetiot, S. Triki, C. J. Gomez-Garcia, *Inorg. Chem.* 2014, **53**, 97-104; (f) A. Galet, M. C. Munoz, J. A. Real, *Inorg. Chem.* 2006, **45**, 4583-4585; (g) S. Hayami, G. Juhász, Y. Maeda, T. Yokoyama, O. Sato, *Inorg. Chem.* 2005, **44**, 7289-7291.
17. SAINT Version 7.68A, Bruker AXS, Inc.; Madison, WI 2009.
18. Sheldrick, G. M. SADABS, Version 2008/1, Bruker AXS, Inc.; Madison, WI 2008.
19. Sheldrick, G. M. SHELXTL, Version 6.14, Bruker AXS, Inc.; Madison, WI 2000-2003.
20. D. Casanova, P. Alemany, J. M. Bofill, S. Alvarez, *Chem. Eur. J.* 2003, **9**, 1281-1295.